

LA-UR-03-5823

Approved for public release;
distribution is unlimited.

Title: TIME SERIES ANALYSIS OF MONTE CARLO FISSION
SOURCES: I. DOMINANCE RATIO COMPUTATION

Author(s): Taro Ueki , Forrest B. Brown,
D. Kent Parsons, and James S. Warsa

Submitted to: Nuclear Science and Engineering,
American Nuclear Society



Los Alamos National Laboratory, an affirmative action/equal opportunity employer, is operated by the University of California for the U.S. Department of Energy under contract W-7405-ENG-36. By acceptance of this article, the publisher recognizes that the U.S. Government retains a nonexclusive, royalty-free license to publish or reproduce the published form of this contribution, or to allow others to do so, for U.S. Government purposes. Los Alamos National Laboratory requests that the publisher identify this article as work performed under the auspices of the U.S. Department of Energy. Los Alamos National Laboratory strongly supports academic freedom and a researcher's right to publish; as an institution, however, the Laboratory does not endorse the viewpoint of a publication or guarantee its technical correctness.

Form 836 (8/00)

Abstract

In the nuclear engineering community, the error propagation of the Monte Carlo fission source distribution through cycles is known to be a linear Markov process when the number of histories per cycle is sufficiently large. In the statistics community, linear Markov processes with linear observation functions are known to have an autoregressive moving average (ARMA) representation of orders p and $p-1$. Therefore, one can perform ARMA fitting of the binned Monte Carlo fission source in order to compute physical and statistical quantities relevant to nuclear criticality analysis. In this work, the ARMA fitting of a binary Monte Carlo fission source has been successfully developed as a method to compute the dominance ratio, i.e., the ratio of the second largest to the largest eigenvalues. The method is free of binning mesh refinement and does not require the alteration of the basic source iteration cycle algorithm. Numerical results are presented for problems with one-group isotropic, two-group linearly anisotropic and continuous energy cross sections. Also, a strategy for the analysis of eigenmodes higher than the second largest eigenvalue is demonstrated numerically.

1. INTRODUCTION

Fitting based on time series analysis is useful for the output analysis in Monte Carlo (MC) simulations. For example, recent work on the confidence interval estimation of the effective neutron multiplication factor (k_{eff}) in MC criticality calculations has demonstrated that autoregressive (AR) fitting performs better than other methods [1-3]. The validity of time series analysis in MC criticality calculations can be argued as follows:

- 1) The sequence of cycle-wise k_{eff} 's is stationary if the stationarity check of the MC fission source is properly performed. The Wold decomposition [4] guarantees that any stationary stochastic process is decomposed into a deterministic part (a singular process with zero prediction error), and a stochastic part (a regular process consisting of the infinite series of uncorrelated noises). Since there is no reason for assuming that cycle-wise k_{eff} 's have a cycle-dependent deterministic part, the Wold decomposition dictates that cycle-wise k_{eff} 's are reduced to the infinite series of uncorrelated noises. On the other hand, AR processes are stationary, have constant mean, and can be reduced to the infinite series of uncorrelated noises. Therefore, AR fitting should approximate the behavior of cycle-wise k_{eff} 's if the order of fitting and the fitting coefficients are appropriately determined.
- 2) For a small natural number p , the autocovariance through the first $p+1$ lags can be evaluated reliably. One can then confine analysis to the stochastic processes with a constraint of the first $p+1$ autocovariances fixed to these evaluated values. The

maximum entropy rate process among these stochastic processes is the p^{th} order AR process by Burg's maximum entropy theorem [5].

The above arguments are elegant and based on established theories. However, they lack algorithm analysis specific to MC criticality calculations.

The error propagation of MC fission source distribution through stationary iteration cycles has been shown to be a linear Markov process driven by uncorrelated noises when the number of histories per cycle is sufficiently large [6]. This Markov process governs the evolution of the fluctuating part of the MC fission source distribution. One can then apply linear operators to that fluctuating part, which defines the observation of fluctuating quantities. Such modeling with evolution and observation separated is much more general than recent modeling on two component systems [7], and the matrix version of the former modeling can be transformed to an ARMA process of orders p and $p-1$ (ARMA($p,p-1$)) [8]. Since ARMA processes are standard stochastic models in time series analysis methods, one can utilize existing numerical libraries or statistics software to analyze output corresponding to various observation functions (matrices). For example, when the observation matrix is the row vector with unity for the j^{th} component and zero otherwise, the output becomes the fluctuating part of the fission source at the j^{th} cell. Also, the eigenvalues of the operator of the aforementioned error propagation have been shown to be the ratio of the nonfundamental to fundamental mode eigenvalues of the original criticality problem [6]. Thus, one is naturally led to speculating that the ARMA fitting of MC fission source is closely connected to higher mode eigenvalue computation.

This article presents one answer to that speculation: the description of a methodology of computing dominance ratio using ARMA fitting. The methodology does not require the alteration of the algorithm of source iteration cycles, as the total number of histories per cycle is fixed and source normalization is performed at each cycle. This is a major difference from recent work on higher mode eigenvalue and eigenfunction computation [9]. Moreover, the methodology is free of mesh-refinement issues because information extraction by the analysis of fluctuation is not compromised by binning mesh sizes. This is an advantage over MC-based fission matrix analysis. Numerical results are presented for problems with one-group isotropic, two-group linearly anisotropic and continuous energy cross sections, where the dominance ratio from ARMA fitting is compared with the dominance ratio computed by deterministic Green's function methods [10], discontinuous finite element discrete ordinate methods [11], asymptotic diffusion analysis [12], or the sphere/slab equivalence formula [13]. Also, the computation of higher modes than the second largest eigenvalue mode is demonstrated numerically.

2. TIME SERIES ANALYSIS OF MC FISSION SOURCE

In this section, the results of previous work on the error propagation of MC fission source [6] are reviewed. These results will then be cast into the form of time series analysis.

2.1. Error Propagation of MC Fission Source

Let $F(\vec{r}' \rightarrow \vec{r})$ be the expected number of the direct descendent particles per unit volume at \vec{r} resulting from a particle born at \vec{r}' . In the case of a position-independent energy spectrum, $F(\vec{r}' \rightarrow \vec{r})$ is the fission kernel defined by the product of energy and angular spectrums, an inverse transport operator and a fission operator, with the last operator defined as $\int \int \nu \Sigma_f(\vec{r}, E) \psi(\vec{r}, E, \vec{\Omega}) d\Omega dE$ for the operand ψ and the fissile descendent generation cross section $\nu \Sigma_f$. The eigenfunctions and eigenvalues of F are denoted by S_j and k_j :

$$S_j(\vec{r}) = \frac{1}{k_j} \int S_j(\vec{r}') F(\vec{r}' \rightarrow \vec{r}) dr' \quad (1)$$

where k_j are ordered as $k_0 > |k_1| > |k_2| > \dots$. The eigenvalue k_j 's are assumed to be discrete.

Note that k_{eff} is the largest eigenvalue k_0 , and S_0 is called the fundamental mode eigenfunction and assumed to be normalized to k_0 :

$$\int S_0(\vec{r}) dr = k_0 = k_{\text{eff}} \quad (2)$$

The fundamental mode eigenvalue k_0 and the effective neutron multiplication factor k_{eff} will be used interchangeably. The normalization condition (2) cannot generally be assumed for S_j , $j \geq 1$ because in symmetric problems the higher-mode eigenfunctions may integrate to zero. In order to simplify later derivations, the following normalization scheme is imposed on the nonfundamental mode eigenfunctions:

$$S_j(\vec{r}) \leftarrow \frac{k_j S_j(\vec{r})}{\int S_j(\vec{r}) dr} \text{ when } \int S_j(\vec{r}) dr \neq 0 \quad (3)$$

i.e., the whole domain integral of $S_j(\vec{r})$ is normalized to the corresponding eigenvalue as far as $\int S_j(\vec{r})dr \neq 0$ and no specification is made otherwise. The source distribution after simulating the m^{th} stationary cycle in a MC criticality calculation can be written as

$$\hat{S}^{(m)}(\vec{r}) = NS(\vec{r}) + \sqrt{N}\hat{\varepsilon}^{(m)}(\vec{r}), m \geq 0, \quad (4)$$

where $\hat{\varepsilon}^{(m)}(\vec{r})$ is the fluctuating component of the stationary source, N the number of particle histories per cycle, the hats indicate a realization of stochastic quantities, and $S(\vec{r})$ is the expected value (ensemble average) of $\hat{S}^{(m)}(\vec{r})/N$. In addition, the random noise component $\hat{\varepsilon}^{(m)}(\vec{r})$ resulting from the starter selection and subsequent particle tracking is introduced as

$$\sqrt{N}\hat{\varepsilon}^{(m)}(\vec{r}) \equiv \hat{S}^{(m)}(\vec{r}) - \frac{N \int F(\vec{r}' \rightarrow \vec{r}) \hat{S}^{(m-1)}(\vec{r}') dr'}{\int \hat{S}^{(m-1)}(\vec{r}'') dr''}. \quad (5)$$

Then, the fluctuating part of the MC fission source becomes a linear Markov process driven by uncorrelated noises with the nonlinear term with the order of $O(N^{-1/2})$ [6]:

$$\hat{\varepsilon}^{(m)}(\vec{r}) = A_0 \hat{\varepsilon}^{(m-1)}(\vec{r}) + \hat{\varepsilon}^{(m)}(\vec{r}) + O(N^{-1/2}), \quad (6)$$

$$E[\hat{\varepsilon}^{(p)} \hat{\varepsilon}^{(q)}] = 0, p > q, \quad (7)$$

$$E[\hat{\varepsilon}^{(p)} \hat{\varepsilon}^{(q)}] = 0, p > q, \quad (8)$$

where A_0 is defined as

$$A_0(\bullet) = \frac{1}{k_0} \int [F(\vec{r}' \rightarrow \vec{r}) - S_0(\vec{r})](\bullet) dr'. \quad (9)$$

The operator A_0 has the following features:

$$A_0^i S_0(\vec{r}) = 0 \quad \text{for } i \geq 1, \quad (10)$$

$$A_0^i [S_j(\vec{r}) - S_0(\vec{r})] = \left(\frac{k_j}{k_0}\right)^i [S_j(\vec{r}) - S_0(\vec{r})] \quad \text{for } j \geq 1 \text{ with } \int S_j(\vec{r}) dr \neq 0 \quad j \geq 1, \quad (11)$$

$$A_0^i S_j(\vec{r}) = \left(\frac{k_j}{k_0}\right)^i S_j(\vec{r}) \quad \text{for } j \geq 1 \text{ with } \int S_j(\vec{r}) dr = 0 \quad j \geq 1. \quad (12)$$

In other words, the operator A_0 maps the fundamental mode eigenfunction in (1) to zero identically and makes the higher mode eigenfunctions in (1) decay by a factor of the ratio of their respective eigenvalue to the fundamental mode eigenvalue. Therefore, the transformation of the system of (6)-(8) to a standard stochastic model may enable one to compute the dominance ratio k_1/k_0 . In the next subsection, we derive an ARMA representation corresponding to the system of (6)-(8).

2.2. Autoregressive Moving Average Representation

First, let us consider the discrete form of (6) and (8) with $O(N^{-1/2})$ terms ignored:

$$\vec{e}^{(m)} = A_0 \vec{e}^{(m-1)} + \vec{\varepsilon}^{(m)}, \quad (13)$$

$$E[\vec{\varepsilon}^{(p)} (\vec{\varepsilon}^{(q)})^t] = 0, \quad (14)$$

where $\vec{e}^{(m)}$ and $\vec{\varepsilon}^{(m)}$ are $p \times 1$ matrices, and A_0 is assumed to be the operator in (9) for functional cases and the corresponding $p \times p$ matrix for discrete cases. In actual MC calculations, the binned source at each cycle subtracted by the sample average of binned sources over cycles yields an estimate of $\vec{e}^{(m)}$. Let us introduce an observation matrix C with p columns:

$$\vec{y}^{(m)} = C \vec{e}^{(m)}. \quad (15)$$

Then, Akaike's theory of Markovian representation of stochastic processes [8] enables one to transform the system of (13) and (14) combined with (15) to an ARMA process. This is a new aspect that is not explored in previous work on discrete models [14, 15].

In order to proceed to ARMA models, the characteristic polynomial of the matrix A_0 is introduced:

$$|\lambda I - A_0| = \lambda^p + \sum_{n=1}^p a_n \lambda^{p-n}, \quad (16)$$

where λ is scalar and I is the identity matrix. The largest root of (16) is assumed to be the dominance ratio k_1/k_0 by Eqs. (10)-(12). This is equivalent to assuming that statistical binning of source distribution preserves the most dominant eigenmode in Eqs. (10)-(12). These aspects will be revisited in Section 3. Also note that stationarity is equivalent to the roots of the characteristic polynomial being inside the unit disk [16]. The Hamilton-Cayley theorem states that the coefficient a 's in (16) satisfy

$$A_0^p + \sum_{n=1}^p a_n A_0^{p-n} = 0. \quad (17)$$

Then, Eq. (15) yields

$$\vec{y}^{(n+p)} + a_1 \vec{y}^{(n+p-1)} + \dots + a_p \vec{y}^{(n)} = C(\vec{e}^{(n+p)} + a_1 \vec{e}^{(n+p-1)} + \dots + a_p \vec{e}^{(n)}) \quad (18)$$

The expression inside the parentheses in the right hand side of Eq. (18) is rewritten, using Eq. (13), as

$$\begin{aligned}
& \bar{e}^{(n+p)} + a_1 \bar{e}^{(n+p-1)} + \dots + a_p \bar{e}^{(n)} \\
&= A_0^p \bar{e}^{(n)} + A_0^{p-1} \bar{\varepsilon}^{(n+1)} + \dots + \bar{\varepsilon}^{(n+p)} + a_1 \left(A_0^{p-1} \bar{e}^{(n)} + A_0^{p-2} \bar{\varepsilon}^{(n+1)} + \dots + \bar{\varepsilon}^{(n+p-1)} \right) + \dots \\
&\quad + a_{p-1} \left(A_0 \bar{e}^{(n)} + \bar{\varepsilon}^{(n+1)} \right) + a_p \bar{e}^{(n)} \tag{19} \\
&= \left(A_0^p + a_1 A_0^{p-1} + \dots + a_p I \right) \bar{e}^{(n)} + \left(A_0^{p-1} + a_1 A_0^{p-2} + \dots + a_{p-1} I \right) \bar{\varepsilon}^{(n+1)} \\
&\quad + \dots + \left(A_0 + a_1 I \right) \bar{\varepsilon}^{(n+p-1)} + \bar{\varepsilon}^{(n+p)}.
\end{aligned}$$

Using Eqs. (17) and (19) and defining

$$E_i = C \left(A_0^i + a_1 A_0^{i-1} + \dots + a_i I \right), \quad E_0 = C, \tag{20}$$

one can rewrite Eq. (18) as

$$\bar{y}^{(n+p)} + a_1 \bar{y}^{(n+p-1)} + \dots + a_p \bar{y}^{(n)} = E_0 \bar{\varepsilon}^{(n+p)} + E_1 \bar{\varepsilon}^{(n+p-1)} + \dots + E_{p-1} \bar{\varepsilon}^{(n+1)}. \tag{21}$$

Eq. (21) is a multivariate ARMA process of order p and $p-1$, denoted by ARMA($p, p-1$).

However, when the observation matrix C is $1 \times p$ row vector, the observation \bar{y} becomes

scalar and the right hand side of Eq. (21) is also scalar. In this case, one can easily

perform a time series analysis of Eq. (21) since many statistical libraries and software

have the routines to analyze scalar ARMA models and/or the least square routines to

compute these model coefficients.

3. DOMINANCE RATIO COMPUTATION

There are two candidates for observation matrices in dominance ratio computation. The

first one produces the fluctuating part of the source at the q^{th} cell:

$$y^{(n)} = \bar{y}^{(n)} = q^{\text{th}} \text{ component of } \bar{e}^{(n)} = C_q \bar{e}^{(n)} = (0, \dots, 0, \underset{q^{\text{th}} \text{ component}}{1}, 0, \dots, 0) \bar{e}^{(n)} \tag{22}$$

The second one produces the fluctuating part of k_{eff} estimates:

$$y^{(n)} = \bar{y}^{(n)} = \text{fluctuating part of } k_{\text{eff}} \text{ estimate} = C_{\text{all}} \bar{e}^{(n)} = (1, 1, \dots, 1) \bar{e}^{(n)}. \quad (23)$$

The observation matrix C_q in (22) is a preferred choice for dominance ratio computation due to the following reasons. The integration of (10)-(12) over the q^{th} cell yields the local modes of the cycle-to-cycle error propagation in the original functional form:

$$\begin{aligned} \int_{q^{\text{th}} \text{ cell}} A_0^i S_0(\vec{r}) dr &= 0, \quad i \geq 1, \\ \int_{q^{\text{th}} \text{ cell}} A_0^i [S_j(\vec{r}) - S_0(\vec{r})] dr &= \left(\frac{k_j}{k_0}\right)^i \int_{q^{\text{th}} \text{ cell}} [S_j(\vec{r}) - S_0(\vec{r})] dr \quad \text{if} \quad \int_{\text{whole domain}} S_j(\vec{r}) dr \neq 0 \text{ and } i \geq 1, \\ \int_{q^{\text{th}} \text{ cell}} A_0^i S_j(\vec{r}) dr &= \left(\frac{k_j}{k_0}\right)^i \int_{q^{\text{th}} \text{ cell}} S_j(\vec{r}) dr \quad \text{if} \quad \int_{\text{whole domain}} S_j(\vec{r}) dr = 0 \text{ and } i \geq 1. \end{aligned} \quad (24)$$

The discrete form of (24) is

$$\begin{aligned} C_q A_0^i \bar{S}_0 &= 0, \quad i \geq 1, \\ C_q A_0^i [\bar{S}_j - \bar{S}_0] &= \left(\frac{k_j}{k_0}\right)^i C_q [\bar{S}_j - \bar{S}_0] \quad \text{if } C_{\text{all}} \bar{S}_j \neq 0 \text{ and } i \geq 1, \\ C_q A_0^i \bar{S}_j &= \left(\frac{k_j}{k_0}\right)^i C_q \bar{S}_j \quad \text{if } C_{\text{all}} \bar{S}_j = 0 \text{ and } i \geq 1. \end{aligned} \quad (25)$$

Using (3), the integration of (10)-(12) over the whole domain yields the global modes of the cycle-to-cycle error propagation in the original functional form:

$$\begin{aligned} \int_{\text{whole domain}} A_0^i S_0(\vec{r}) dr &= 0, \quad i \geq 1, \\ \int_{\text{whole domain}} A_0^i [S_j(\vec{r}) - S_0(\vec{r})] dr &= k_0 \left(\frac{k_j}{k_0}\right)^i \left(\frac{k_j}{k_0} - 1\right) \int_{\text{whole domain}} S_j(\vec{r}) dr \neq 0 \text{ and } i \geq 1, \\ \int_{\text{whole domain}} A_0^i S_j(\vec{r}) dr &= 0 \quad \text{if} \quad \int_{\text{whole domain}} S_j(\vec{r}) dr = 0 \text{ and } i \geq 1. \end{aligned} \quad (26)$$

The discrete equivalent to (26) is

$$\begin{aligned}
C_{all} A_0^i \vec{S}_0 &= 0, i \geq 1, \\
C_{all} A_0^i [\vec{S}_j - \vec{S}_0] &= k_0 \left(\frac{k_j}{k_0} \right)^i \left(\frac{k_j}{k_0} - 1 \right) \quad \text{if } C_{all} \vec{S}_j \neq 0 \text{ and } i \geq 1, \\
C_{all} A_0^i S_j &= 0 \quad \text{if } C_{all} \vec{S}_j = 0 \text{ and } i \geq 1.
\end{aligned} \tag{27}$$

The repeated application of (13) yields

$$\vec{e}^{(m)} = \sum_{i=0}^{m-1} A_0^i \vec{e}^{(m-i)} + A_0^{m-1} \vec{e}^{(0)}, \tag{28}$$

where $\vec{e}^{(0)}$ stands for the fluctuating part of the source at the last inactive cycle.

Therefore, under the assumption that the \vec{e} 's and $\vec{e}^{(0)}$ can be expanded by the eigenvectors \vec{S}_j , Eqs. (27) and (28) imply that the factor $k_0(k_j/k_0 - 1)$ makes the ARMA fitting of the fluctuating part of $k_{\text{eff}}(C_{all}\vec{e}^{(m)})$ hopeless when the dominance ratio k_1/k_0 is close to unity. On the other hand, the cancellation effect resulting from the factor $k_0(k_j/k_0 - 1)$ and the complete cancellation in the third equation of (27) (or (26)) do not exist in Eq. (25) (or (24)). Therefore, the ARMA fitting of the fluctuating part of the fission source at the q^{th} cell ($C_q\vec{e}^{(m)}$) is much more favorable against the ARMA fitting of $C_{all}\vec{e}^{(m)}$. Moreover, we choose the simplest source binning; binary cells $q=1,2$ ($p=2$). This should work if one is interested in computing only dominance ratio (k_1/k_0) because, in general, $C_q[\vec{S}_1 - \vec{S}_0] \neq 0$ and $C_q\vec{S}_1 \neq 0$, and one can overlay several different sets of binary cells.

When the ARMA(p,p-1) process in (21) is scalar (C is $1 \times p$ matrix), its lag i autocovariance $\gamma(i)$ satisfies [16]:

$$\gamma(i) + a_1\gamma(i-1) + \dots + a_p\gamma(i-p) = 0, i \geq p. \quad (29)$$

The general solution of Eq. (29) (see, e.g., Appendix A4.1 in Ref. [16]) is known to be

$$\gamma(i) = b_1\lambda_1^i + b_2\lambda_2^i + \dots + b_p\lambda_p^i, i \geq p, \quad (30)$$

where $|\lambda_1| > \dots > |\lambda_p|$ are the roots of the characteristic polynomial (16). Since the term $b_1\lambda_1^p$ becomes dominant for large lags, the fitted coefficients yield an accurate estimate of λ_1 if the number of samples, i.e., active cycles in MC criticality calculations, is sufficiently large. On the other hand, (28), (7) and (8) yield

$$\begin{aligned} & \text{lag } i \text{ autocovariance of the } q^{\text{th}} \text{ cell} \\ &= \frac{1}{N} E \left[\int_{q^{\text{th}} \text{ cell}} \int_{q^{\text{th}} \text{ cell}} \hat{e}^{(m+i)}(\vec{r}) \hat{e}^{(m)}(\vec{r}') dr dr' \right] \\ &= \frac{1}{N} \sum_{j=0}^{m-1} E \left[\int_{q^{\text{th}} \text{ cell}} A_0^{i+j} \hat{\mathcal{E}}^{(m-j)}(\vec{r}) \int_{q^{\text{th}} \text{ cell}} A_0^j \hat{\mathcal{E}}^{(m-j)}(\vec{r}') dr' \right] \\ &+ \frac{1}{N} E \left[\int_{q^{\text{th}} \text{ cell}} A_0^{i+m} \hat{e}^{(0)}(\vec{r}) dr \int_{q^{\text{th}} \text{ cell}} A_0^m \hat{e}^{(0)}(\vec{r}') dr' \right] + O(N^{-3/2}), \end{aligned} \quad (31)$$

where the first equality is due to stationarity. Assuming that m is sufficiently large ($m \gg 1$), which is valid when the number of observations (stationary cycles computed) is much larger than the decay of the geometric power of k_1/k_0 , Eq. (31) can be rewritten as

$$\begin{aligned} & \text{lag } i \text{ autocovariance of the } q^{\text{th}} \text{ cell} \\ &\cong \frac{1}{N} \sum_{j=0}^{m-1} E \left[\int_{q^{\text{th}} \text{ cell}} A_0^{i+j} \hat{\mathcal{E}}^{(m-j)}(\vec{r}) \int_{q^{\text{th}} \text{ cell}} A_0^j \hat{\mathcal{E}}^{(m-j)}(\vec{r}') dr' \right] + O(N^{-3/2}). \end{aligned} \quad (32)$$

Moreover, Eqs. (10)–(12), the completeness assumption of S_j , $j = 0, 1, \dots$ and the previous assumption of $m \gg 1$ enable one to rewrite (32) in the following form:

$$\begin{aligned} & \text{lag } i \text{ autocovariance of the } q^{\text{th}} \text{ cell} \\ &\cong \frac{1}{N} \left[B_1 \left(\frac{k_1}{k_0} \right)^i + B_2 \left(\frac{k_2}{k_0} \right)^i + B_3 \left(\frac{k_3}{k_0} \right)^i + \dots \right] + O \left(N^{-\frac{3}{2}} \right), \end{aligned} \quad (33)$$

where B 's are constant with respect to i and m , and Eq. (24) implies that B 's are proportional to the following quantity:

$$B_j \propto \begin{cases} \int_{\text{q-th cell}} [S_j(\vec{r}) - S_0(\vec{r})] dr & \text{if } \int_{\text{whole domain}} S_j(\vec{r}) dr \neq 0, \\ \int_{\text{q-th cell}} S_j(\vec{r}) dr & \text{if } \int_{\text{whole domain}} S_j(\vec{r}) dr = 0. \end{cases} \quad (34)$$

Comparing (30) with (33), one may conclude that if the number of observations is sufficiently large, $\lambda_1 = k_1 / k_0$ (dominant modes) and k_j / k_0 ($j = 2, 3, \dots$) are lumped together into $\lambda_2, \dots, \lambda_p$. This is the reason we focus our effort on computation of the dominance ratio. Eq. (30) also indicates that if $\lambda_1^p = (k_1 / k_0)^p \ll 1$, the dominance ratio computed by ARMA(p,p-1) fitting would have large statistical uncertainty.

The parameters of ARMA models can be estimated by least-squares methods. [16] Since these least-squares methods have been firmly established and are in use in the field of time series analysis, we utilize the IMSL statistical library [17] to compute the coefficients and covariance matrix of the ARMA(2,1) fitting of the MC binary fission source. The ARMA(2,1) representation is

$$\begin{aligned} y^{(n+2)} + a_1 y^{(n+1)} + a_2 y^{(n)} &= E_0 \vec{\epsilon}^{(n+2)} + E_1 \vec{\epsilon}^{(n+1)}, \\ E_0 &= C_q, \\ E_1 &= C_q (A_0 + a_1 I). \end{aligned} \quad (35)$$

The characteristic polynomial (16) of the ARMA(2,1) representation (35) is

$$\lambda^2 + a_1 \lambda + a_2 = 0. \quad (36)$$

The dominance ratio is estimated as the larger of the roots of (36):

$$\lambda_+ = -\frac{a_1}{2} + \sqrt{\frac{a_1^2}{4} - a_2} . \quad (37)$$

We always perform the stationarity diagnostics of the MC fission source distribution [6,18] before attempting an ARMA(2,1) fitting because stationarity is equivalent to the absolute value of the roots of the characteristic polynomial being smaller than unity [16].

The variance of the dominance ratio is estimated as

$$\begin{aligned} \text{var}(\lambda_+) &= \left(\frac{\partial \lambda_+}{\partial a_1}\right)^2 \text{var}(a_1) + \left(\frac{\partial \lambda_+}{\partial a_2}\right)^2 \text{var}(a_2) + 2\left(\frac{\partial \lambda_+}{\partial a_1}\right)\left(\frac{\partial \lambda_+}{\partial a_2}\right) \text{cov}(a_1, a_2) \\ &= \left(-\frac{1}{2} + \frac{a_1}{2\sqrt{a_1^2 - 4a_2}}\right)^2 \text{var}(a_1) + \frac{1}{a_1^2 - 4a_2} \text{var}(a_2) \\ &\quad + \frac{2}{\sqrt{a_1^2 - 4a_2}} \left(\frac{1}{2} - \frac{a_1}{2\sqrt{a_1^2 - 4a_2}}\right) \text{cov}(a_1, a_2). \end{aligned} \quad (38)$$

4. NUMERICAL RESULTS – DOMINANCE RATIO

In this section, numerical results are presented for systems with one-group isotropic, two-group linearly anisotropic and continuous energy cross sections. Stationarity check with relative entropy [6,18] has been performed for all computations to ensure that cycle-wise binned source data come from stationary cycles. The word “active cycles” in this and later sections is meant to imply that the computation has passed the stationarity check.

4.1 One dimensional slab with one-group isotropic scattering cross sections

The first problem involves loosely-coupled one-dimensional slabs with one-group isotropic scattering cross sections investigated in previous work:

Problem 1-1

- 5 region slab, with void boundary conditions on both sides and one-group isotropic cross sections,
- the regions are (left to right) 1.0, 1.0, 5.0, 1.0, and 1.0 cm thickness,
- the materials are (left to right) 2 (fuel), 1 (scatterer), 3 (absorber), 1, and 2,
- material 1 (scatterer)

$$\Sigma_{total} = 1.0 \text{ cm}^{-1}, \Sigma_{scattering} = 0.8 \text{ cm}^{-1}, \Sigma_{capture} = 0.2 \text{ cm}^{-1},$$

- material 2 (fuel)

$$\Sigma_{total} = 1.0 \text{ cm}^{-1}, \Sigma_{scattering} = 0.8 \text{ cm}^{-1}, \Sigma_{capture} = 0.1 \text{ cm}^{-1}, \Sigma_{fission} = 0.1 \text{ cm}^{-1}, \nu = 3.0,$$

- material 3 (absorber)

$$\Sigma_{total} = 1.0 \text{ cm}^{-1}, \Sigma_{scattering} = 0.1 \text{ cm}^{-1}, \Sigma_{capture} = 0.9 \text{ cm}^{-1}.$$

Problem 1-2

- Same as problem 1-1 except the rightmost slab has a thickness of 1.01 cm.

The binary source binning boundary is set up at the middle of the central absorber slab in both problems. Sixty thousand (60000) active cycles of sixty thousand (60000) histories are computed for these problems. Table I shows the dominance ratio appeared in previous work [19] computed by deterministic Green's function methods [10] and an ARMA(2,1) fitting. Results from both methods agree within statistical uncertainty. The large

statistical error of Problem 1–2 is observed to be about four times that of Problem 1–1. This appears to be caused by a significantly large distortion in the fission source distribution of loosely coupled systems; the fission source of Problem 1-2 is about 0.97 to 0.03 for the rightmost slab to the leftmost slab.

4.2 Two dimensional checkerboard with one-group isotropic scattering cross sections

The second problem involves a two-dimensional heterogeneous system:

Problem 2

- Two dimensional checkerboard with size and cross sections shown in Figure 1.

Forty thousand active cycles of eighty thousand histories are computed for this problem. Figure 2 shows a dominance ratio computed by an ARMA(2,1) fitting and estimated by the analysis of the spectral radius of outer iterations in discontinuous finite element discrete ordinates methods [11]. It is observed that the results from ARMA(2,1) fitting agree with the estimation by discontinuous finite element discrete ordinates methods regardless of binning meshes. Figure 3 shows a dominance ratio computed by AR(1)=ARMA(1,0), and AR(2)=ARMA(2,0), and an ARMA(2,1) fitting, where $a_2 = 0$ (fixed) and $E_1 = 0$ (fixed) in AR(1) and $E_1 = 0$ (fixed) in AR(2). Both AR(1) and AR(2) are observed to be reasonably good approximations in this problem.

4.3 Three dimensional homogeneous cube with one-group isotropic scattering cross sections

The third problem is a three dimensional homogeneous cube system with one-group isotropic cross sections:

Problem 3

- Three dimensional cube with various sizes.
- Cross sections are $\Sigma_t = 1.0 \text{ cm}^{-1}$, $\Sigma_s = 0.75 \text{ cm}^{-1}$, $\Sigma_a = 0.25 \text{ cm}^{-1}$, $\nu\Sigma_f = 0.275 \text{ cm}^{-1}$.

Forty thousand active cycles of eighty thousand histories are computed for each size of the cubes. The binary binning boundary is set up at $z=0$ for the domain $|x|<D$, $|y|<D$, and $|z|<D$, where D is the half length of the cube side. Figure 4 shows a dominance ratio computed by an ARMA(2,1) fitting, evaluated by discontinuous finite element discrete ordinates methods and asymptotic diffusion analysis [12]:

$$\text{dominance ratio of homogeneous cube} \cong \frac{k_{eff}}{k_{infinity}}, \quad (39)$$

where $k_{infinity}$ is calculated for the same cross sections. Eq. (39) is expected to yield a good estimate for large homogeneous cubes. The dominance ratio by the ARMA(2,1) fitting is observed to be in good agreement with the deterministically evaluated dominance ratio.

A small statistical error is observed for the large cubes. This can be explained as follows:

The large size implies a small leakage through the exterior surfaces and small communication through the binary binning boundary compared to the number of histories

per cycle. This causes strongly positive correlation over sources at adjacent cycles ($\bar{y}^{(n+1)}$ and $\bar{y}^{(n)}$ in (35)). To offset that effect, the coefficients a_1 and a_2 are strongly negatively correlated. For example, the correlation coefficient of a_1 and a_2 is larger than -0.95 in magnitude for larger sizes than 70 cm. On the other hand, strong positive correlation of $\bar{y}^{(n+2)}$ and $\bar{y}^{(n+1)}$ implies that these centered binary sources fluctuate to the same side with respect to their common mean (zero). This also implies that a_1 is negative and the coefficient of the cross term in (38) becomes positive. Therefore, the cross term in (38) becomes large and negative, and the variance of the dominance ratio estimate λ_+ becomes small for large cubes.

4.4 One dimensional homogeneous slab with linearly-anisotropic two-group cross sections

The fourth problem is a critical U-D₂O slab [20]:

Problem 4

- Critical U-D₂O slab of thickness 1858.9 cm.
- Linearly-anisotropic two-group cross sections (See Table II).

Forty thousand active cycles of thirty thousand histories were computed on the MCNP5 code [21]. The binary binning boundary is set up at the center of the slab. The result in Table III shows that the dominance ratio by an ARMA(2,1) fitting agrees with the evaluation by discontinuous finite element discrete ordinates methods.

4.5 One dimensional homogeneous slab with continuous energy cross sections

The fifth problem has continuous energy cross sections:

Problem 5

- Homogeneous slab of various sizes.
- Continuous energy cross sections for 8 g/liter Pu-239 in a water solution.

Since deterministic methods are not available for continuous energy cross section systems, the dominance ratio computed by an ARMA(2,1) and an AR(2) fitting is compared with two approximate methods. One method is the asymptotic diffusion analysis [12]:

$$\text{dominance ratio of homogeneous slab} \cong \left(\frac{k_{eff}}{k_{infinity}} \right)^3, \quad (40)$$

and another method is a sphere-slab equivalence formula that is valid for any homogeneous slab with isotropic scattering [13]:

$$\text{dominance ratio of slab with thickness } D \cong \frac{k_{eff}(\text{sphere of diameter } D)}{k_{eff}(\text{slab of thickness } D)}, \quad (41)$$

where both k_{eff} in (41) are for the same cross section systems as the original slab problem.

Five thousand active cycles of ten thousand histories are computed for the $k_{infinity}$ and sphere problems, and ten thousand active cycles of ten thousand histories are computed for the slab problems. Both of these computations were implemented on the MCNP5

code [21]. The binary binning boundary is set up at the center of each slab. Figure 5 shows the dominance ratio computed by the ARMA(2,1) fitting of the slab problems and the approximations in (40) and (41). The standard deviation of dominance ratio computed by (40) and (41) is the order of the fifth fractional digit, which is too small to be shown as error bars. Therefore, error bars are shown for only the ARMA(2,1) fitting results. All three methods are observed to agree well for sizes larger than or equal to 100 cm. Figure 6 shows the dominance ratio computed by the AR(2) fitting. It is observed that the performance of the AR(2) fitting is as good as the analytic diffusion approximation in (40). Combining the results from Figures 3, 5 and 6, one may hope that the AR(2) fitting performs as well as diffusion approximations. Also, as observed and discussed in Subsection 4.3, the statistical error of the dominance ratio is small for large slabs.

5. NUMERICAL RESULTS – HIGHER MODES

5.1. Symmetric Problem

As the ARMA fitting of k_{eff} was dismissed in Section 3, Eq. (34) implies that if the integral of the first mode cancels out over the q^{th} cell and over the (entire) domain, which is sometimes the case in symmetric problems, one cannot compute the dominance ratio through the ARMA(2,1) fitting of the source at the q^{th} cell. Eq. (34) also implies that if the integral of the second mode over the q^{th} cell does not cancel out and the integral of the first mode cancels out over the q^{th} cell and over the (entire) domain, one can compute the second to fundamental mode eigenvalue ratio k_2 / k_0 through the ARMA(2,1) fitting

of the source at the q^{th} cell. This is because for the q^{th} cell so chosen, $B_1 = 0$ in Eq. (34), and therefore the coefficients a_1 and a_2 resulting from actual ARMA(2,1) fitting yield $\lambda_1 = k_2 / k_0$, the new dominant mode in Eq. (33). Similarly, if the integrals of the first and second modes cancel out over the q^{th} cell and over the (entire) domain, but the integral of the third mode over the q^{th} cell does not cancel out, one can compute the third to fundamental mode eigenvalue ratio k_3 / k_0 through the ARMA(2,1) fitting of the source at the q^{th} cell. To demonstrate these strategies, we have analyzed a huge homogeneous cube with the same cross sections as those of Problem 3.

Problem 6

- Cube with side length of 200 cm,
- Cross sections are the same as those of Problem 3.

Table IV shows the nonfundamental to fundamental mode eigenvalue ratio for the first through third modes computed by the ARMA(2,1) fitting, where thirty-six thousand active cycles of fifty thousand histories are computed. Table V shows the first through third mode eigenvalues computed by the discontinuous finite element discrete ordinates method with Krylov subspace iterations [22]. Table V also contains the first through third to fundamental mode eigenvalue ratios by the straightforward extension of the asymptotic diffusion analysis in Ref. [12]:

$$\left(\begin{array}{l} \text{nonfundamental to fundamental} \\ \text{mode eigenvalue ratio} \end{array} \right) \cong \left(\frac{k_{eff}}{k_{infinity}} \right)^n, \quad (42)$$

where $n = 1, 2$, and $8/3$ for the first, second, and third mode, respectively [23]. It is observed that all the ARMA(2,1) fitting results contain the discontinuous finite element discrete ordinates results within statistical uncertainty.

We have also analyzed a huge homogeneous sphere problem.

Problem 7

- Sphere with radius of 100 cm.
- Cross sections are the same as those of Problem 3.

Since

$$\nabla^2 = \frac{1}{r^2} \left[\frac{\partial}{\partial r} r^2 \frac{\partial}{\partial r} + \frac{\partial}{\partial \mu} (1 - \mu^2) \frac{\partial}{\partial \mu} + \frac{1}{1 - \mu^2} \frac{\partial^2}{\partial \varphi^2} \right],$$

where μ is the cosine of the polar angle θ and φ is the azimuthal angle, asymptotic diffusion analysis (assuming the separation of radial and angular variables for space representation) dictates that the eigenfunctions of a homogeneous sphere take the following form:

$$\begin{aligned} & \frac{\sin(\pi(R_L + 1)r/R)}{r} \\ & \times \begin{cases} P_{N_S}^{M_S}(\mu) \cos(M_S \varphi), & M_S = 0, \dots, N_S, \\ P_{N_S}^{|M_S|}(\mu) \sin(|M_S| \varphi), & M_S = -1, \dots, -N_S, \end{cases} \quad R_L = 0, 1, \dots, \text{ and } N_S = 0, 1, \dots, \end{aligned} \quad (43)$$

where $0 \leq r < R$, $-1 \leq \mu \leq 1$, $0 \leq \varphi < 2\pi$, and $P_{N_S}^{M_S}$ is the associated Legendre function

[24]. The angular part of (43) denoted here by Y_{N_S, M_S} satisfies

$$\left[\frac{\partial}{\partial \mu} (1 - \mu^2) \frac{\partial}{\partial \mu} + \frac{1}{1 - \mu^2} \frac{\partial^2}{\partial \varphi^2} \right] Y_{N_S, M_S} = -N_S(N_S + 1) Y_{N_S, M_S},$$

because the associated Legendre function satisfies

$$\frac{\partial}{\partial \mu} (1 - \mu^2) \frac{\partial}{\partial \mu} P_{N_s}^{M_s} - \frac{M_s^2}{1 - \mu^2} P_{N_s}^{M_s} + N_s (N_s - 1) = 0.$$

Therefore, the eigenmodes have a multiplicity of $2N_s + 1$. Table VI shows the fundamental and next five eigenmodes computed by the discontinuous finite element discrete ordinates method with Krylov subspace iterations. In the MC simulation, forty thousand cycles of forty thousand histories were computed with various overlaid binary meshes. Table VII shows the first through third to fundamental mode eigenvalue ratio computed by the ARMA(2,1) fitting. It is observed that the results from discrete ordinates and MC methods agree within statistical uncertainty. To compute the fourth to fundamental mode eigenvalue ratio, two subcells were combined with multipliers as shown in Table VIII.

These multipliers are determined by

$$\left(\frac{k_3}{k_0} \right) \frac{\int_0^{0.5} \frac{\sin(2\pi r)}{r} r^2 dr}{\int_0^1 \frac{\sin(2\pi r)}{r} r^2 dr} - \frac{\int_0^{0.5} \frac{\sin(\pi r)}{r} r^2 dr}{\int_0^1 \frac{\sin(\pi r)}{r} r^2 dr} = -0.816,$$

$$\left(\frac{k_3}{k_0} \right) \frac{\int_{0.5}^1 \frac{\sin(2\pi r)}{r} r^2 dr}{\int_0^1 \frac{\sin(2\pi r)}{r} r^2 dr} - \frac{\int_{0.5}^1 \frac{\sin(\pi r)}{r} r^2 dr}{\int_0^1 \frac{\sin(\pi r)}{r} r^2 dr} = 0.812,$$

in order to cancel out the third mode error propagation expressed in the second equations of (24) and (25). Note that the factor k_3/k_0 results from (3). This two-subcell combination corresponds to the following observation matrix:

$$C = (0, \dots, 0, 0.812, 0.816, 0, \dots, 0).$$

Note that the angular integrals $\int_0^\pi \left[\int_0^{\pi/3} + \int_{2\pi/3}^\pi + \int_{4\pi/3}^{5\pi/3} \right] (\bullet) d\varphi d\theta$ and

$\int_0^\pi \left[\int_{-\pi/6}^{\pi/6} + \int_{\pi/2}^{5\pi/6} + \int_{7\pi/6}^{3\pi/2} \right] (\bullet) d\varphi d\theta$ cancel out the first and second mode error propagation

expressed in the third equations of (24) and (25). Also note that Eq. (6) holds for

$c(\vec{r})\hat{e}(\vec{r})$ and $c(\vec{r})\hat{\varepsilon}(\vec{r})$ instead of $\hat{e}(\vec{r})$ and $\hat{\varepsilon}(\vec{r})$ if $c(\vec{r})$ is a cell-wise constant

function. It is observed that the corresponding results in Tables VI and VIII agree within

statistical uncertainty. To compute the fifth to fundamental mode eigenvalue ratio, four

subcells were combined in a multilevel manner as shown in Table IX. In order to cancel

out the first, second, and fourth mode error propagation expressed in the third equations

of (24) and (25), the multipliers -1.01 and 2.17 are determined by

$$\int_0^{0.5} \frac{\sin(\pi r)}{r} r^2 dr = 1.01 \quad \text{and} \quad \int_{0.5}^{1.0} \frac{\sin(\pi r)}{r} r^2 dr = 2.17.$$

The multipliers 1 and -1 for the next level cell combination cancel out the third mode

error propagation expressed in the second equations of (24) and (25) because of the

rotational symmetry of that mode. These multipliers correspond to the following

observation matrix:

$$C = (1, -1) \begin{pmatrix} 2.17, & -1.01, & 0, & 0 \\ 0, & 0, & 2.17, & -1.01 \end{pmatrix}.$$

It is observed that the corresponding results in Tables VI and IX agree within statistical

uncertainty.

5.2 A Realistic Application – PWR Fuel Storage Facility

At first glance, the computational strategy in Section 5.1 appears to be restrictive.

However, many challenging problems in criticality safety and reactor physics consist of loosely coupled components/subdomains, which may allow one to assume the separation of the horizontal-plane and vertical-direction modes. Once such separation is assumed, one can attempt to compute an eigenvalue ratio for the first and second modes. For example, if a fitted cell spans over the whole horizontal domain, the ARMA(2,1) fitting of that cell yields the eigenvalue ratio of the mode for the vertically first and horizontally fundamental mode. The vertically fundamental and horizontally first mode can be computed by the fitting of a cell spanning over the whole vertical domain. Note that Eq. (10) holds for the vertically and horizontally fundamental mode. Moreover, realistic problems usually have some symmetry. This can be further utilized to compute the eigenvalue ratio for the third or higher modes.

To demonstrate these strategies, we have analyzed a PWR fuel storage facility:

Problem 8

- A checkerboard array of fuel bundles and water lattices surrounded by water and concrete investigated in the OECD/NEA Working Party on Nuclear Criticality Safety, Expert Group on Source Convergence Analysis [25].
- Geometry and materials are shown in Figure 7.
- All fuel bundles are fresh; the pellet density is 0.06925613 atoms/b-cm, and $U_{238} : O : U_{235} = 2.238 : 4.6054 : 0.082213$.

Since concrete is a superior reflector to water, the fission source distribution has a large peak at the (1,3) lattice location as shown in Figure 8. Here one should note a similarity between Problems 1 and 8. Problem 1-2 corresponds to Problem 8 and Problem 1-1 to Problem 8 with the rightmost column in the checkerboard removed. The fission source distribution is 0.5:0.5 for Problem 1-1 and 0.03:0.97 for Problem 1-2. The statistical error of their dominance ratio is 0.00027 for Problem 1-1 and 0.00102 for Problem 1-2 when their binary binning boundary is placed at the middle of the central absorber slab. The fission source distribution in Figure 8 is more skewed to the left than the 0.03:0.97 skewness. Therefore, the binary binning boundary in Problem 8 should not be placed between the 12th and 13th columns. Table X shows the statistical error of dominance ratio for different binary binning boundaries. One clearly sees the increase of standard deviation as the binary binning boundary moves to the right. Table XI shows the dominance ratio for the vertically fundamental mode and the largest two eigenvalue ratios for the horizontally fundamental mode. It is observed that the vertically second and horizontally fundamental mode is statistically evaluated to be smaller than the vertically first and horizontally fundamental mode and the vertically fundamental and horizontally first mode. The vertically fundamental and horizontally first mode is evaluated to be smaller than the vertically first and horizontally fundamental mode within statistical uncertainty of two standard deviations.

6. A REMARK ON COMPLEX HIGHER-MODE EIGENVALUES IN CONTINUOUS-ENERGY CROSS-SECTION PROBLEMS

The authors of this article are aware of no literature that has proved that all eigenvalues of continuous-energy cross-section problems are real. Thus, we briefly mention what kinds of statistical properties of the MC fission source would be associated with the existence of complex higher mode eigenvalues. Suppose that λ_1 and λ_2 as well as b_1 and b_2 in Eq. (30) are complex conjugates:

$$\begin{aligned}
\lambda_1 &= \lambda_R + \lambda_I \mathbf{i} = \sqrt{\lambda_R^2 + \lambda_I^2} e^{i\theta}, \\
\lambda_2 &= \lambda_R - \lambda_I \mathbf{i} = \sqrt{\lambda_R^2 + \lambda_I^2} e^{-i\theta}, \\
b_1 &= b_R + b_I \mathbf{i} = \sqrt{b_R^2 + b_I^2} e^{i\varphi}, \\
b_2 &= b_R - b_I \mathbf{i} = \sqrt{b_R^2 + b_I^2} e^{-i\varphi}.
\end{aligned} \tag{44}$$

The autocovariance of lag j would then become

$$\gamma(j) = 2\sqrt{b_R^2 + b_I^2} (\lambda_R^2 + \lambda_I^2)^{\frac{j}{2}} \cos(\varphi + j\theta) + b_3 \lambda_3^j + \dots + b_p \lambda_p^j, \quad j \geq p. \tag{45}$$

Therefore, when the autocorrelation of a MC fission source is dominated by sinusoidal decay, the first and second mode eigenvalues may be complex. We have not yet discovered such a continuous-energy cross-section problem.

7. A REMARK ON MACMILLAN'S FORMULA FOR CONFIDENCE INTERVAL ESTIMATION

Eq. (33) has the same form as the expression of autocovariance that MacMillan [26] first assumed in order to derive a quick fix-up formula for the confidence interval estimations in iterated source calculations. Eq. (30) is the corresponding expression in ARMA(p,p-1) models. Both of these expressions consist of the sum of geometric powers. Therefore, the

ARMA($p,p-1$) fitting of source could also be developed as an improvement to the confidence interval estimation in MC criticality calculations.

8. CONCLUSIONS

The ARMA(2,1) fitting of the MC binary fission source has been successfully developed as a method to compute the dominance ratio. The method can also be applied to the computation of modes higher than the second largest eigenvalue mode. All the results by ARMA(2,1) fitting have been successfully tested against reference results computed by established deterministic methods, except for continuous-energy cross-section problems. The ARMA(2,1)-based dominance ratio computation is free of binning mesh refinement issues. In other words, information extraction by the analysis of fluctuation through ARMA(2,1) fitting is not compromised by binning mesh size. This may encourage the future study of other statistical analysis methods of eigenmodes like principal component analysis.

REFERENCES

1. L. Demaret et al., "Accurate Determination of Confidence Intervals in Monte Carlo Eigenvalue Calculations," *Proc. 6th Int. Conf. Nuclear Criticality Safety*. Versailles, France, September 20-24, (1999).
2. O. Jacquet et al., "Eigenvalue Uncertainty Evaluation in MC Calculation, Using Time Series Methodologies," *Advanced Monte Carlo for Radiation Physics, Particle Transport Simulation and Applications, Proc. Monte Carlo 2000 Conf.*, Lisbon, Portugal, October 23-26, 2000. A. Kling et al., Eds., Springer-Verlag, Berlin, Heidelberg (2001).
3. T. Ueki and F.B. Brown, "Autoregressive Fitting for Monte Carlo K-effective Confidence Intervals," *Trans. Am. Nucl. Soc.*, **86**, 210 (2002).
4. M.B. Priestley, *Spectral Analysis and Time Series*, Eighth Edition, Academic Press, London UK (1994).
5. T.M. Cover and J.A. Thomas, *Elements of Information Theory*, John Wiley & Sons, New York (1991).
6. T. Ueki, F.B. Brown, D.H. Parsons and D.E. Kornreich, "Autocorrelation and Dominance Ratio in Monte Carlo Criticality Calculations," accepted for publication in *Nuclear Science and Engineering* (2003).
7. T. Yamamoto, T. Nakamura and Y. Miyoshi, "Fission Source Convergence of Monte Carlo Criticality Calculations in Weakly Coupled Fissile Arrays," *Journal of Nuclear Science and Technology*, **37**, pp.41-52 (2000).

8. H. Akaike, "Markovian Representation of Stochastic Processes and Its Application to the Analysis of Autoregressive Moving Average Processes," *Annals of the Institute of Statistical Mathematics*, **26**, 363 (1974).
9. T.E. Booth, "Computing the Higher k-eigenfunctions by Monte Carlo Power Iteration: A conjecture," *Nucl. Sci. Eng.*, **143**, 291 (2003).
10. D.E. Kornreich and B.D. Ganapol, "The Green's Function Method for Nuclear Engineering Applications," *Nucl. Sci. Eng.*, **126**, 293 (1997). (Also see D. E. Kornreich and D. K. Parsons, "The Green's Function Method of Effective Multiplication Benchmark Calculations in Multi-Region Slab Geometry," accepted for publication in *Annals of Nuclear Energy* (2003).)
11. T.A. Wareing, J.M. McGhee, J.E. Morel and S.D. Pautz, "Discontinuous Finite Element S_N Methods on Three-dimensional Unstructured Grids," *Nucl. Sci. Eng.*, **138**, 256 (2001)
12. D.K. Parsons and D.E. Kornreich, "Approximations to the Dominance Ratio Using Effective and Infinite Multiplication Results," in the proceedings of *Nuclear Mathematical and Computational Sciences: A Century In Review – A Century Anew*, M&C 2003, April 6-10, 2000, Gatlinburg, Tennessee.
13. B. Davison, *Neutron Transport Theory*, Oxford, Clarendon Press (1957).
14. R.J. Brissenden and A.R. Garlick, "Biases in the Estimation of Keff and Its Error by Monte Carlo Methods," *Annals of Nuclear Energy*, **13**, 2, 63 (1986).
15. E.M. Gelbard and A.G. Gu, "Biases in Monte Carlo Eigenvalue Calculations," *Nucl. Sci. Eng.*, 117, 1 (1994).

16. G.E.P. Box, G.M. Jenkins and G.C. Reinsel, *Time Series Analysis: Forecasting and Control*, Prentice-Hall, Inc., Upper Saddle River, New Jersey (1994).
17. *IMSL Stat/Library Volume 2*, Visual Numerics, Inc., Houston Texas (1997).
18. T. Ueki and F.B. Brown, "Stationarity and Source Convergence Diagnostics in Monte Carlo Criticality Calculations," in the proceedings of *Nuclear Mathematical and Computational Sciences: A Century In Review – A Century Anew*, M&C 2003, April 6-10, 2000, Gatlinburg, Tennessee.
19. D.E. Kornreich and D.K. Parsons, "Semi-analytic Results and Insights into Difficult Source Convergence Problems," *Trans. Am. Nucl. Soc.*, **87**, 152 (2002).
20. A. Sood, R.A. Forster, and D.K. Parsons, "Analytical Benchmark Test Set For Criticality Code Verification," *Progress in Nuclear Energy*, **42**, 1, 55 (2003).
21. X-5 Monte Carlo Team, "MCNP – A General Purpose Monte Carlo N-Particle Transport Code, Version 5," , Los Alamos National Laboratory report LA-UR-03-1987, Los Alamos, NM (April, 2003).
22. J.S. Warsa, T.A. Wareing, J.E. Morel, J.M. McGhee, and R.B. Lehoucq, "Krylov Subspace Iterations for the Calculation of k -eigenvalues with S_N Transport Codes," in the proceedings of *Nuclear Mathematical and Computational Sciences: A Century In Review – A Century Anew*, M&C 2003, April 6-10, 2000, Gatlinburg, Tennessee.
23. D.K. Parsons and D.E. Kornreich, private communication, 2003.
24. G.B. Folland, *Fourier Analysis and Its Applications*, Brooks/Cole Pub. Co., Pacific Grove, CA (1992).
25. R.N. Blomquist and A. Nouri, "The OECD/NEA Source Convergence Benchmark Problem," *Trans. Am. Nucl. Soc.*, **87**, 143 (2002).

26. D.B. MacMillan, "Monte Carlo Confidence Limits for Iterated-source Calculations,"

Nucl. Sci. Eng., **50**, 73 (1973).

Table I: Dominance ratio of Problems 1 computed by deterministic Green's function methods (GFM) and ARMA(2,1) fitting.

	Problem 1-1	Problem 1-2
GFM	0.99957	0.99250
ARMA(2,1)	$0.99944 \pm 0.00027^*$	$0.9921 \pm 0.0010^*$

* two standard deviations

Table II: Cross-section data for Problem 4

Fast energy group cross-sections* for linearly anisotropic scattering (cm ⁻¹)									
Material	ν_2	Σ_{2f}	Σ_{2c}	Σ_{22s0}	Σ_{22s1}	Σ_{12s0}	Σ_{12s1}	Σ_{2t}	χ_2
UD ₂ O	2.50	0.0028172	0.0087078	0.31980	0.06694	0.004555	-0.0003972	0.33588	1.0
Slow energy group cross-sections* for linearly anisotropic scattering (cm ⁻¹)									
Material	ν_1	Σ_{1f}	Σ_{1c}	Σ_{11s0}	Σ_{11s1}	Σ_{21s}	Σ_{1t}	χ_1	
UD ₂ O	2.50	0.097	0.02518	0.42410	0.05439	0.0	0.54628	0.0	

* group 2 is the fast group and group 1 is the slow group

Table III: Dominance ratio of Problem 4 computed by discontinuous finite element discrete ordinates methods and ARMA(2,1) fitting.

	ARMA(2,1)	discontinuous finite element S_n
Dominance ratio	$0.9989 \pm 0.0005^*$	0.9993

* two standard deviations

Table IV: Nonfundamental to fundamental mode eigenvalue ratio of Problem 6 computed by ARMA(2,1) fitting

Mode	Eigenvalue	ARMA(2,1) fitting	
		Ratio	Fitted cell** (one cell in binary binning)
fundamental	$1.09894 \pm 0.00002^*$	1	N/A
first	N/A	$0.99933 \pm 0.00038^*$	$0 < x$
second	N/A	$0.99781 \pm 0.00069^*$	$[(x < 0, y < 0) \text{ or } (0 < x, 0 < y)]$
third	N/A	$0.99773 \pm 0.00072^*$	$ x < 33.3$

* two standard deviations

** Domain is assumed to be $-100 < x < 100$, $-100 < y < 100$, $-100 < z < 100$

Table V: First ten eigenvalues of Problem 6 computed by discontinuous finite-element discrete-ordinate method with Krylov subspace iterations

Mode	Asymptotic diffusion analysis		Discontinuous finite element S_N	
	Mode	Ratio	Eigenvalue	Ratio
Fundamental	$\cos(1)-\cos(1)-\cos(1)$	1	1.09893	1
first	$\sin(2)-\cos(1)-\cos(1)$	0.99903	1.09787	0.99903
	$\cos(1)-\sin(2)-\cos(1)$			
	$\cos(1)-\cos(1)-\sin(2)$			
second	$\cos(1)-\sin(2)-\sin(2)$	0.99806	1.09681	0.99807
	$\sin(2)-\cos(1)-\sin(2)$			
	$\sin(2)-\sin(2)-\cos(1)$			
third	$\cos(1)-\cos(1)-\cos(3)$	0.99741	1.09611	0.99743
	$\cos(1)-\cos(3)-\cos(1)$			
	$\cos(3)-\cos(1)-\cos(1)$			

Table VI: First twenty eigenvalues of Problem 7 computed by discontinuous finite element discrete ordinates method with Krylov subspace iterations

Mode	Asymptotic diffusion analysis (radial & spherical-harmonic mode)	S_N	
		Eigenvalue	Ratio
fundamental	$R_L = 0, N_S = 0, M_S = 0$	1.09858	1
first	$R_L = 0, N_S = 1, M_S = -1, 0, 1$	1.09710	0.99866
second	$R_L = 0, N_S = 2, M_S = -2, -1, 0, 1, 2$	1.09525	0.99697
third	$R_L = 1, N_S = 0, M_S = 0$	1.09436	0.99616
fourth	$R_L = 0, N_S = 3, M_S = -3, -2, -1, 0, 1, 2, 3$	1.09305	0.99497
fifth	$R_L = 1, N_S = 1, M_S = -1, 0, 1$	1.09153	0.99359

Table VII: Nonfundamental to fundamental mode eigenvalue ratio of Problem 7 computed by ARMA(2,1) fitting

Mode	Eigenvalue	ARMA(2,1) fitting	
		Ratio	Fitted cell** (one cell in binary binning)
fundamental	$1.09857 \pm 0.00002^*$	1	N/A
first	N/A	$0.99886 \pm 0.00044^*$	$0 \leq r < 100, 0 \leq \theta \leq \pi, 0 \leq \varphi < \pi.$
second	N/A	$0.99659 \pm 0.00077^*$	$0 \leq r < 100, 0 \leq \theta \leq \pi,$ $[0 < \varphi < 0.5\pi \text{ or } \pi < \varphi < 1.5\pi]$
third	N/A	$0.99612 \pm 0.00082^*$	$0 \leq r < 50, 0 \leq \theta \leq \pi, 0 \leq \varphi < 2\pi$

* two standard deviations

** Domain is assumed to be $0 \leq r < 100$ (radial), $0 \leq \theta \leq \pi$ (polar), $0 \leq \varphi < 2\pi$ (azimuthal).

Table VIII: Fourth to fundamental mode eigenvalue ratio of Problem 7 computed by ARMA(2,1) fitting

Combined cells for fitting**			Eigenvalue ratio
Combination scheme	Subcell	Multiplier	
1	$0 \leq r < 50, 0 \leq \theta \leq \pi,$ $[0 < \varphi < \pi/3$ or $2\pi/3 < \varphi < \pi$ or $4\pi/3 < \varphi < 5\pi/3]$	0.812	$0.9949 \pm 0.0014^*$
	$50 \leq r < 100, 0 \leq \theta \leq \pi,$ $[0 < \varphi < \pi/3$ or $2\pi/3 < \varphi < \pi$ or $4\pi/3 < \varphi < 5\pi/3]$	0.816	
2	$0 \leq r < 50, 0 \leq \theta \leq \pi,$ $[-\pi/6 < \varphi < \pi/6$ or $\pi/2 < \varphi < 5\pi/6$ or $7\pi/6 < \varphi < 3\pi/2]$	0.812	$0.9944 \pm 0.0014^*$
	$50 \leq r < 100, 0 \leq \theta \leq \pi,$ $[-\pi/6 < \varphi < \pi/6$ or $\pi/2 < \varphi < 5\pi/6$ or $7\pi/6 < \varphi < 3\pi/2]$	0.816	

* two standard deviations

** Domain is assumed to be $0 \leq r < 100$ (radial), $0 \leq \theta \leq \pi$ (polar), $0 \leq \varphi < 2\pi$ (azimuthal).

Table IX: Fifth to fundamental mode eigenvalue ratio of Problem 7 computed by ARMA(2,1) fitting

Combined cells for fitting**				Eigenvalue ratio
Multiplier		Multiplier		0.9927 ± 0.0012*
1		-1		
Subcell	Multiplier	Subcell	Multiplier	
$0 < \theta < \pi, 0 < \varphi < \pi,$ $0 < r < 50$	2.17	$0 < \theta < \pi, \pi < \varphi < 2\pi,$ $0 < r < 50$	2.17	
$0 < \theta < \pi, 0 < \varphi < \pi,$ $50 < r < 100$	-1.01	$0 < \theta < \pi, \pi < \varphi < 2\pi,$ $50 < r < 100$	-1.01	

* two standard deviations

** Domain is assumed to be $0 \leq r < 100$ (radial), $0 \leq \theta \leq \pi$ (polar), $0 \leq \varphi < 2\pi$ (azimuthal).

Table X: Standard deviation of dominance ratio of Problem 8 computed by horizontal binary binning (50000 histories per cycle and 7000 active cycles)

Bin	$0 < x < 27$ cm $54 < y < 81$ cm ((1,3) lattice)	$x < 81$ cm (column 1-4)	$x < 162$ cm (column 1-7)	$x < 324$ cm (column 1-12)
Standard Deviation	0.0007	0.0011	0.0013	0.0025

Table XI: Nonfundamental to fundamental mode eigenvalue ratio of Problem 8 computed by ARMA(2,1) fitting (20000 active cycles of 60000 histories per cycle)

Mode		ARMA(2,1) fitting	
Horizontal	Vertical	Eigenvalue ratio	Fitted cell (one cell in binary binning)
first	fundamental	$0.9930 \pm 0.0016^*$	$0 < x < 27, 54 < y < 81, -180 < z < 180.$
fundamental	first	$0.9959 \pm 0.0012^*$	$0 < x < 648, 0 < y < 81, 0 < z < 180.$
fundamental	second	$0.9807 \pm 0.0027^*$	$0 < x < 648, 0 < y < 81, -60 < z < 60.$

* two standard deviations

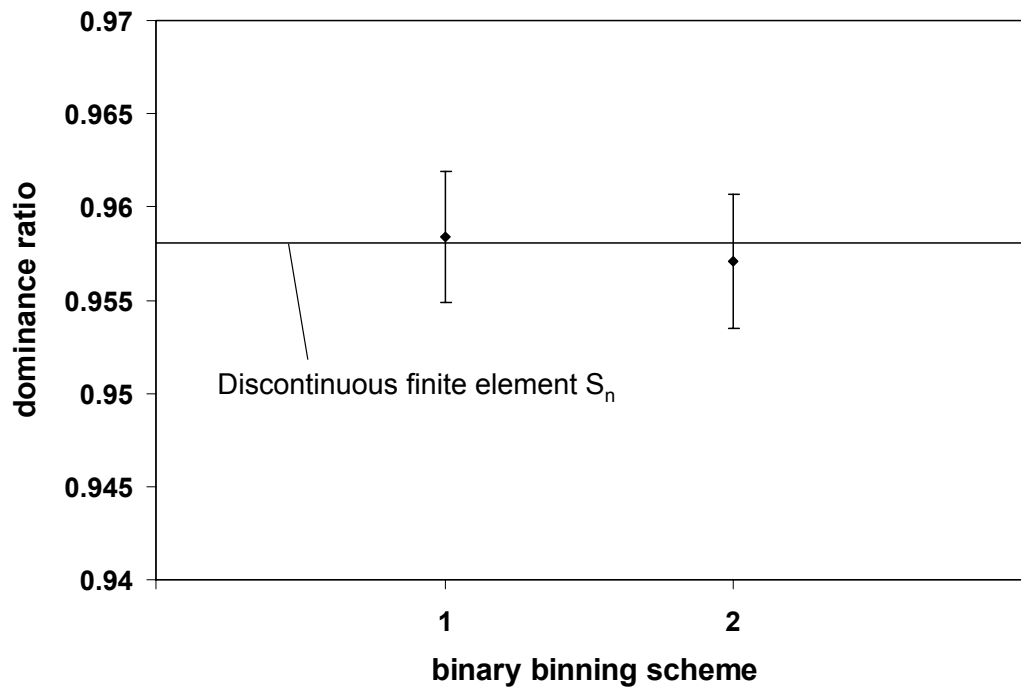


Figure 2: Dominance ratio of Problem 2 by ARMA(2,1)
(two standard deviations for half length of error bars)

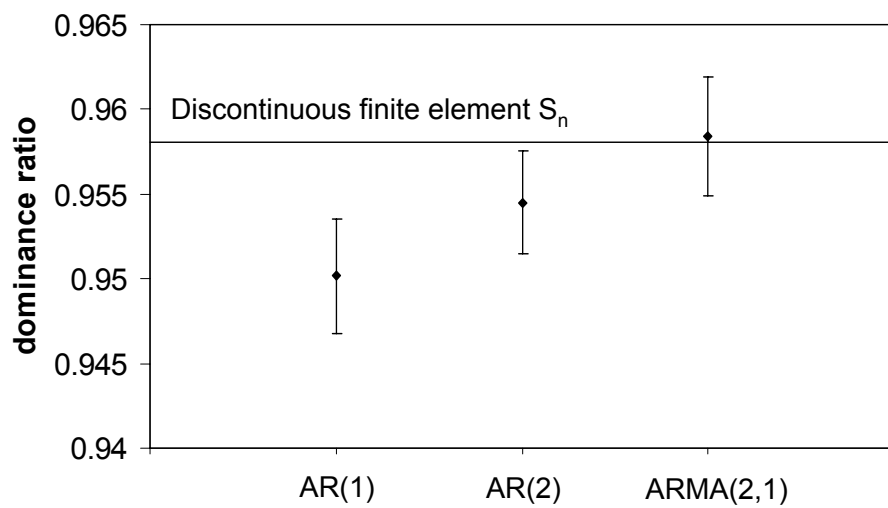


Figure 3: Dominance ratio of Problem 2 by AR(1), AR(2), and ARMA(2,1) fitting of binning scheme 1 (two standard deviations for half length of error bars)

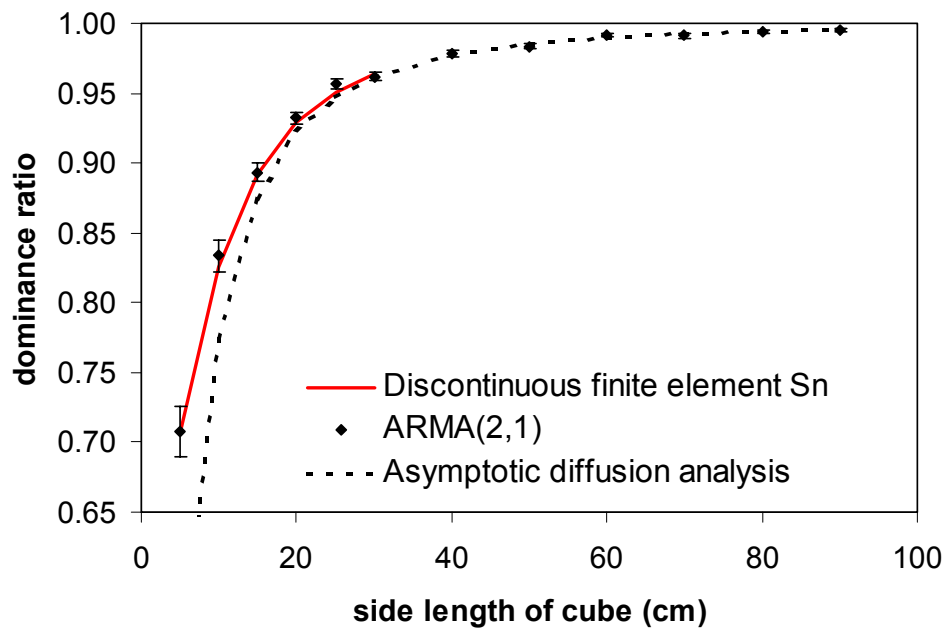


Figure 4: Dominance ratio of Problem 3
(two standard deviations for half length of error bars)

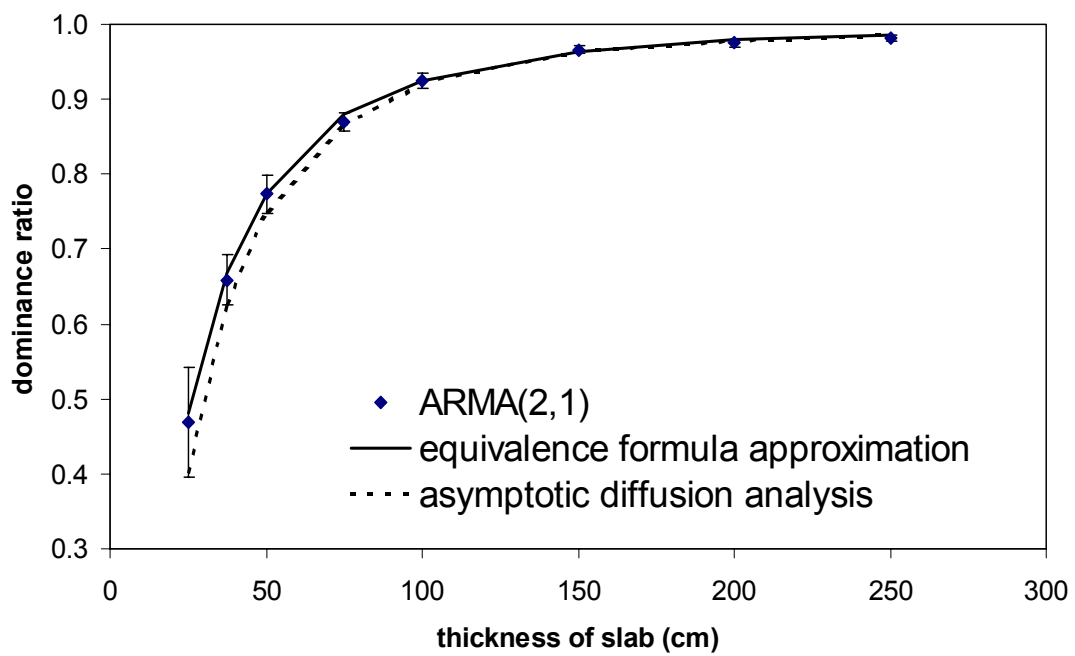


Figure 5: Dominance of Problem 5
 (two standard deviations for half length of error bars)

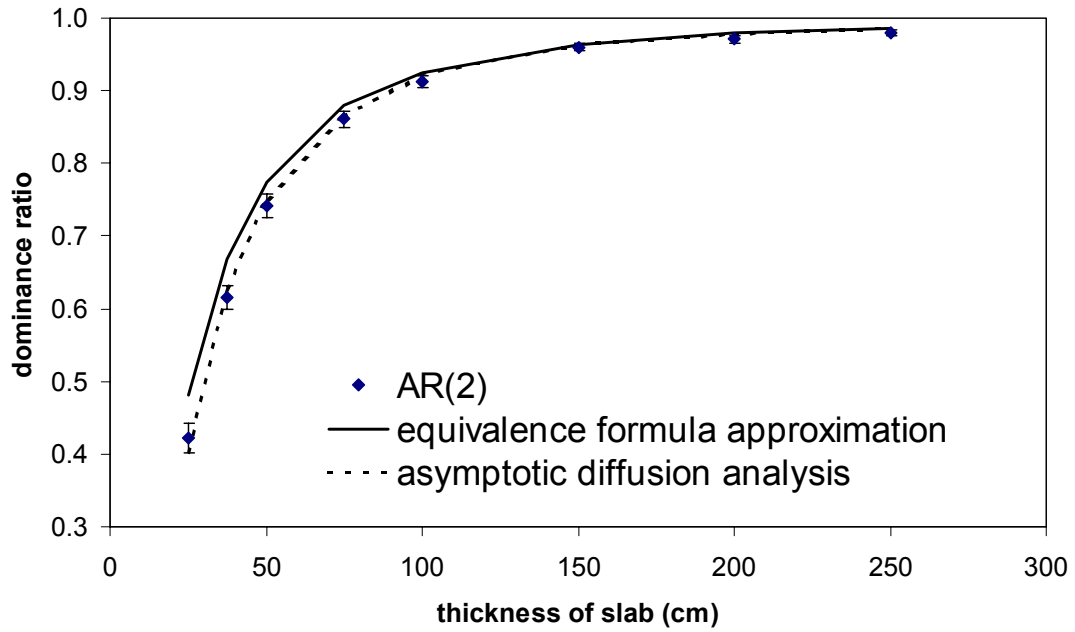
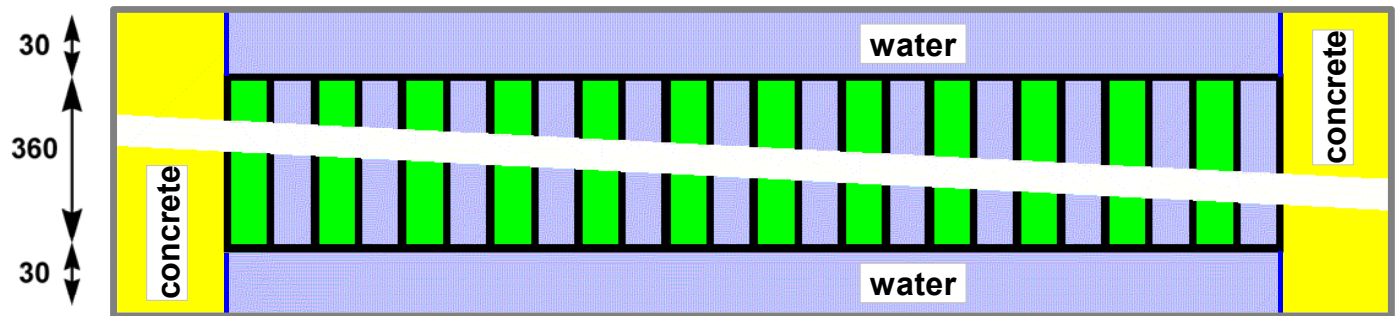
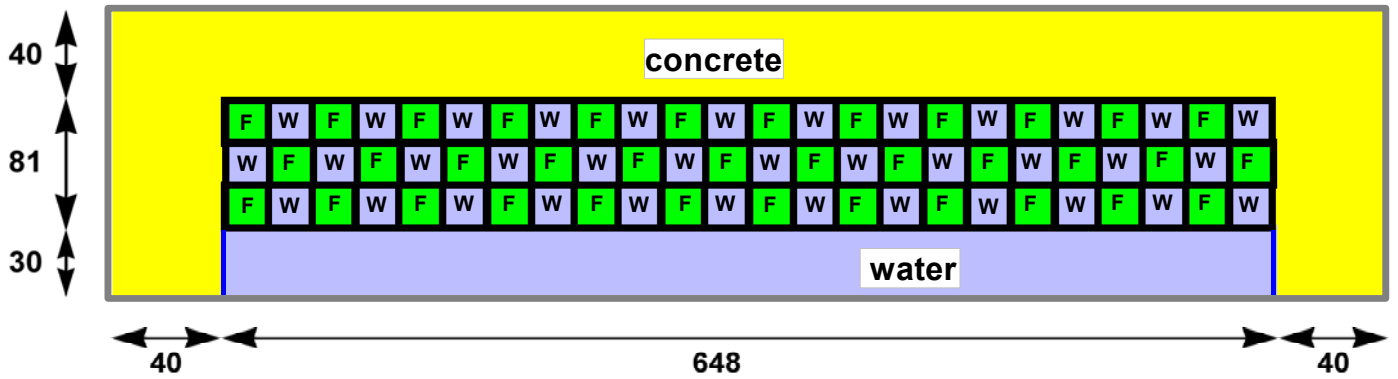


Figure 6: Dominance ratio of Problem 5 by AR(2) approximation (two standard deviations for half length of error bars)

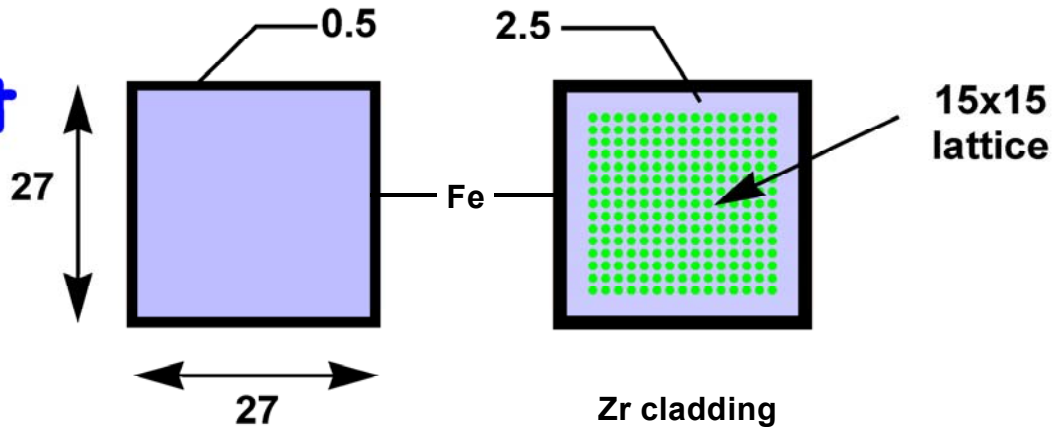
Top View

F = fuel bundle, W = water



Side View

Element Details



All dimensions in cm

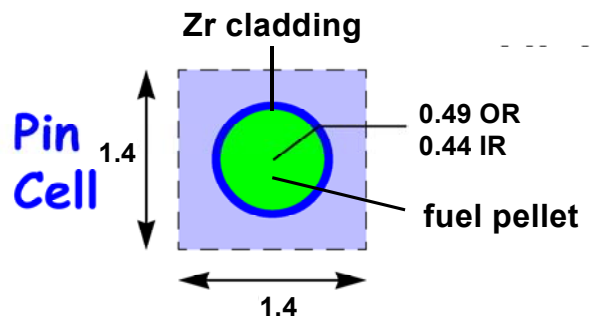


Figure 7: Geometry and materials in Problem 8

Columns 17-24

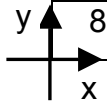
119		60		7		2	
	72		25		2		4
55		22		5		2	

Columns 9-16

568		343		193		222	
	361		235		177		129
314		158		128		98	

Columns 1-8

40531		11070		3887		1201	
	15665		5519		1922		712
8279		5285		1951		679	



(normalized to sum = 100000)

Figure 8: Average of stationary fission source distributions (arbitrary units)